Probing Lysozyme Conformation with Light Reveals a New Folding Intermediate†

Andrea C. Hamill, Shao-Chun Wang, and C. Ted Lee, Jr.*

Department of Chemical Engineering, University of Southern California, Los Angeles, California 90089-1211

Received August 18, 2005; Revised Manuscript Received September 20, 2005

ABSTRACT: A means to control lysozyme conformation with light illumination has been developed using the interaction of the protein with a photoresponsive surfactant. Upon exposure to the appropriate wavelength of light, the azobenzene surfactant undergoes a reversible photoisomerization, with the visible-light (trans) form being more hydrophobic than the UV-light (cis) form. As a result, surfactant binding to the protein and, thus, protein unfolding, can be tuned with light. Small-angle neutron scattering (SANS) measurements were used to provide detailed information of the protein conformation in solution. Shape-reconstruction methods applied to the SANS data indicate that under visible light the protein exhibits a native-like form at low surfactant concentrations, a partially swollen form at intermediate concentrations, and a swollen/unfolded form at higher surfactant concentrations. Furthermore, the SANS data combined with FT-IR spectroscopic analysis of the protein secondary structure reveal that unfolding occurs primarily in the α domain of lysozyme, while the β domain remains relatively intact. Thus, the surfactant-unfolded intermediate of lysozyme appears to be a separate structure than the well-known α-domain intermediate of lysozyme that contains a folded α domain and unfolded β domain. Because the interactions between the photosurfactant and protein can be tuned with light, illumination with UV light returns the protein to a native-like conformation. Fluorescence emission data of the nonpolar probe Nile red indicate that hydrophobic domains become available for probe partitioning in surfactant−protein solutions under visible light, while the availability of these hydrophobic domains to the probe decrease under UV light. Dynamic light scattering and UV−vis spectroscopic measurements further confirm the shape-reconstruction findings and reveal three discrete conformations of lysozyme. The results clearly demonstrate that visible light causes a greater degree of lysozyme swelling than UV light, thus allowing for the protein conformation to be controlled with light.

The biological *function* of a protein is largely determined by the *structure* of the protein, and thus, much work has been aimed at investigating this form−function relationship. The method of choice in this regard has been X-ray crystallography, which has been shown to be quite successful at elucidating the structure of soluble proteins in the native state. However, the form−function relationship is not static in nature, and instead, it is often necessary for the protein to adopt non-native or partially folded conformations to perform certain functions, whether beneficial (e.g., enzymatic catalysis, transport across cellular membranes, immune protection, etc.) or harmful [e.g., ailments such as Alzheimer's disease, cystic fibrosis, Mad Cow disease, amyloid diseases, prion diseases, and even many cancers are believed to result from misfolded proteins (*1*, *2*)]. In the specific case of lysozyme, mutations of the protein have been found to produce structural transitions that lead to amyloidosis (*3*), with large quantities, sometimes kilograms, of aggregated protein accumulating in organs such as the liver, kidney, and spleen (*4*, *5*).

Despite the fact that intermediately folded states represent key structures along folding pathways, high-resolution structural information of unfolded or partially folded states is limited, largely because intermediately folded proteins typically aggregate over the long times required for crystallization, a result of exposure of the hydrophobic regions of the protein to solvent (*6*). Thus, developing novel methods of investigating intermediate states in solution, as opposed to in the crystalline form, is warranted. However, direct high-resolution structural studies of these intermediates are usually precluded because of their transient nature (lifetimes < 100 ms), thereby relegating the investigation of these *kinetic intermediates* primarily to the field of simulations (*7*, *8*), although novel experimental strategies have been developed to study the folding process, such as time-resolved small-angle X-ray scattering, nuclear magnetic resonance (NMR),[1] and various spectroscopic techniques combined with stopped-flow methods (*9*−*12*). An alternate approach is to study *equilibrium intermediates*, partially folded states stabilized by selected solvents, denaturants, or surfactants, because a variety of evidence suggests that equilibrium intermediates

† We acknowledge the Charles Lee Powell Foundation for support of this research.

* To whom correspondence should be addressed. Telephone: (213) 740-2066. Fax: (213) 740-8053. E-mail: tedlee@usc.edu.

[1] Abbreviations: azoTAB, azobenzene-trimethylammonium bromide; BSA, bovine serum albumin; CD, circular dichroism; CTAB, cetyltrimethylammonium bromide; DLS, dynamic light scattering; FT-IR, Fourier transform infrared spectroscopy; R_H, hydrodynamic radius; NMR, nuclear magnetic resonance spectroscopy; PDB, Protein Data Bank; PDDF, pair distance distribution function; R_g, radius of gyration; SANS, small-angle neutron scattering; SDS, sodium dodecyl sulfate; UV−vis, UV−visible spectroscopy.

10.1021/bi051646c CCC: $30.25
Published on Web 10/29/2005

are similar in conformation to the corresponding kinetic intermediates (*13*−*20*). In this manner, "snapshots" along the protein-folding pathway can be stabilized as equilibrium intermediates, allowing an investigation of the mechanisms of protein folding.

It is generally observed that c-type lysozymes do not exhibit intermediately folded states during equilibrium folding experiments (*21*), except for extreme conditions such as low pH or when mixed with a solvent. In kinetic folding experiments, however, a populated intermediate has been observed (*22*−*25*). Upon initiating refolding from the denatured state, lysozyme rapidly (within a few milliseconds) forms an ensemble of different hydrophobically collapsed states (*11*). After this rapid collapse, the majority of the molecules (∼70%) accumulate into a stable kinetic intermediate, often termed the α-intermediate (I_α), with a structured α domain and disordered β domain. The rate-limiting step for formation of the native state is then refolding of the β domain, allowing formation of the hydrophobic interface between the α and β domains, with molecular dynamics simulations (*26*) and mutation studies (*27*−*29*) suggesting that the final step in the folding process may be insertion of the β-domain residues Leu-55 and Ile-56 into a hydrophobic pocket of the α domain. Of the remaining 30% of molecules that do not fold via the formation of the I_α intermediate, $\sim^2/_3$ fold very rapidly as the α and β domains form simultaneously ($I_{\alpha/\beta}$ intermediate), while $^1/_3$ fold very slowly, potentially limited by a cis−trans isomerization of proline.

The manner in which a protein folds depends upon the interplay between electrostatic, hydrogen-bonding, van der Waals, and hydrophobic interactions among the amino acid residues making up the protein. In the native state, the charged and polar amino acid groups typically reside on the exterior of the protein exposed to water, while the nonpolar amino acid groups are largely found inside the folded structure of the protein, protected from unfavorable solvent interactions. Protein unfolding can then be induced to different extents by changing variables such as pH, temperature, pressure, or through the addition of a chemical denaturant (i.e., urea or GdmCl) (*13*, *15*). Surfactants have also been shown to unfold proteins (*19*, *20*), including lysozyme, where the hydrophobic moieties of the surfactant cause unfolding by interacting with nonpolar amino acids, thereby eliminating unfavorable solvent contacts. Because surfactant hydrophobicity increases as the length of the hydrocarbon tail increases, it has been found that a greater degree of protein unfolding occurs with increased surfactant molecular weight for a given headgroup (*30*).

In a previous study, it was shown that with the use of a photoresponsive surfactant ("azoTAB"), simple light illumination could be used to induce reversible changes in the conformation of proteins (*19*). An azobenzene group in the hydrocarbon tail allowed the surfactant hydrophobicity to be tuned with light, with the visible-light (trans) isomer being more hydrophobic and thus having a higher affinity to bind to proteins than the UV-light (cis) form. Small-angle neutron scattering (SANS) data combined with *shape-reconstruction techniques* (to be discussed below) were used to determine the structure of bovine serum albumin (BSA) in solution, and three conformations of the protein were observed. At low surfactant concentrations, the native, heart-shaped structure (*N* form) of BSA was evident. However, upon increasing the azoTAB concentration under visible light, the C-terminal portion of the protein was seen to separate from the molecule, giving rise to a partially unfolded intermediate structure (*F* form). This unfolding mechanism had been suspected on the basis of indirect evidence (e.g., UV−vis, CD, and FT-IR) (*31*), now "visualized" from the SANS data. As the surfactant concentration was further increased under visible light, a highly unfolded/elongated conformation (*E* form) was detected, although a significant α-helical content still remained, which was observed as "kinks" in the protein chain from the shape-reconstructed SANS fits. It was also shown that light illumination could be used to reversibly switch between these folded forms.

In the present study, we demonstrate that intermediately folded states of lysozyme can be stabilized in solution with the azoTAB surfactant and that light illumination can be used to induce changes between these conformations. SANS, dynamic light scattering (DLS), FT-IR, UV−visible, and fluorescence spectroscopic measurements are performed on the lysozyme−azoTAB system to investigate the folding of the protein. At low surfactant concentrations, native-like structures of lysozyme are observed, while increasing the azoTAB concentration under visible light causes the α domain of the protein to swell, resulting in a partially unfolded structure at intermediate surfactant concentrations, and to eventually form a swollen/unfolded form of lysozyme at high concentrations. Under UV light at all azoTAB surfactant concentrations, however, the protein appears to be in a native-like state; thus, light can be used to manipulate the protein, allowing for reversible control of protein folding.

MATERIALS AND METHODS

Materials. An azobenzene-trimethylammonium bromide surfactant (azoTAB) of the form

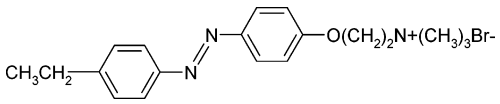

similar to the surfactant used in a previous study (*19*), was synthesized according to published procedures (*32*, *33*) via an azo-coupling reaction of 4-ethlyalaniline with phenol subsequently followed by reactions with 1,2-dibromoethane and finally trimethylamine. The surfactant undergoes a photoisomerization when illuminated with UV light that is fully reversible with the exposure to visible light (*19*, *34*). The visible-light form of the surfactant is primarily in the trans state (75:25 trans/cis ratio), while the UV-light form is mostly in the cis state (>90% cis) (*34*). Photoisomerization with exposure to light changes the dipole moment across the −N═N− bond in the surfactant. The visible-light (trans, planar) form of the surfactant has a lower dipole moment and is therefore more hydrophobic than the UV-light (cis, bent) form, resulting in the UV-light form having a higher affinity for water and the visible-light form a higher affinity for protein binding.

Two illumination methods were used for surfactant photoisomerization. For DLS, FT-IR, and UV−visible spectroscopy, conversion to the cis form was achieved with the 365 nm line from a 200 W mercury arc lamp (Oriel, Stratford, CT, model number 6283), isolated with the combination of

a 320 nm band passfilter (Oriel, model number 59 800) and a heat-absorbing filter (Oriel, model number 59 060). A 400-nm long passfilter (Oriel, model number 59 472) was used to convert back to the trans form. Before measurements, solutions were illuminated with this lamp for at least 10 min. For FT-IR and DLS, light exposure was continued throughout the entire collection of data (hours) by directly illuminating the samples using a liquid light guide (Oriel, model number 77 557). In the small-angle neutron scattering and fluorescence spectroscopy experiments, the solutions were exposed to an 84 W long wave UV lamp, 365 nm (Spectroline, Westbury, NY, model number XX-15A), for at least 30 min to convert to the cis form; to convert back to the trans form, the samples were simply left in room light. For the neutron scattering experiments, the samples were continuously exposed to the same UV light throughout the data collection (to maintain the cis form). Note that 365 nm corresponds to UV-A radiation, as opposed to UV-C, which is know to inactivate lysozyme (*35*). Control experiments confirmed that neither UV nor visible light affected the structure of lysozyme (ΔA < 1% throughout the amide I region from FT-IR).

Highly purified and lyophilized hen-egg-white lysozyme (catalog number L-7651) and a low ionic strength phosphate buffer (pH 7.2, 8.3 mM) were purchased from Sigma; all other chemicals were obtained from Aldrich in the highest purity. Because of the relatively small size of lysozyme, a protein concentration of 11.8 mg/mL was used in the neutron scattering measurements to achieve a reasonable scattering intensity (e.g., each spectra took ~4 h to collect). Additionally, higher protein concentrations were not studied to avoid the formation of lysozyme dimers, which are well-known to begin to form beyond this concentration at neutral pH. For DLS (and subsequent UV−vis) experiments, a protein concentration of 1.0 mg/mL was employed to approximate the diffusion coefficient at infinite dilution.

SANS. The neutron scattering data were collected on the 30-m NG-3 SANS instruments at NIST (*36*) using a neutron wavelength of $\lambda = 6$ Å. Two sample−detector distances were used, 1.33 and 7.0 m, with a detector offset of 25 cm to produce a Q range of 0.0048−0.46 Å^{-1}, where $Q = 4\pi\lambda^{-1}\sin(\theta/2)$ and θ is the scattering angle. The net intensities were corrected for the background and empty cell (pure D_2O), followed by accounting for the detector efficiency using the scattering from an isotropic scatterer (Plexiglas) and then converted to an absolute differential cross section per unit sample volume (in units of cm^{-1}) using an attenuated empty beam. The incoherent scattering intensities from the hydrogen atoms in lysozyme (0.004 cm^{-1}) and the surfactant (0−0.0012 cm^{-1}) were subtracted from the experimental intensities to obtain the coherent scattering from each sample.

The SANS data were analyzed using several complementary techniques to develop consistent conclusions and to cross-check the data, including Guinier analysis, a shape-reconstruction algorithm, and calculation of the pair distance distribution functions (PDDFs). The shape reconstructions were performed using the GA_STRUCT program (*37*). The data files are fit by treating the protein as a collection of 1000 spherical scattering centers, the positions of which were adjusted until the simulated data agreed with the experimental data. The Q range used for the data fits was $0.01 < Q < 0.3$ Å^{-1}. This range was used to exclude potential protein interactions that would be exhibited at low Q and to avoid length scales too small for protein continuity at high Q.

The PDDF is a measure of the probability $P(r)$ of finding two scattering centers at a distance r apart (*38*, *39*); thus, information about protein conformation can be readily obtained from the PDDF using a model-independent, straightforward procedure. PDDFs were calculated assuming a monodisperse system using GNOM (*40*) over a Q range of 0.02−0.3 Å^{-1}, again to exclude interactions at low Q. The maximum particle diameter, D_{max}, was selected to be the lowest value that gave a smooth return of the PDDF to 0 at D_{max}.

DLS. DLS measurements were performed at 25 °C on a Brookhaven model BI-200SM instrument (Brookhaven Instrument Corp., Holtsville, NY) with a 35 mW (Melles Griot, Carlsbad, CA, model number 05-LHP-928) helium neon (λ = 632.8 nm) laser. The scattered light was collected at an angle of 30° to decrease Q and, hence, increase the decay time, thereby allowing the full correlation function, even for a small protein such as lysozyme, to be observed. The laser wavelength was high enough to not convert the azoTAB cis isomer into the trans form during the course of the experiments, thus, allowing long sample times (up to 120 min). The data were analyzed with both the NNLS and CONTIN routines (difference < 2 Å) using a BI-9000AT digital correlator (Brookhaven Instrument Corp.). Before each measurement, the protein−surfactant solutions were passed through a 0.2 μm PVDF filter and then through a 0.02 μm Anatop filter. UV−vis spectra were taken after filtration to determine both the surfactant and protein concentrations. The experimental results represent the average obtained from two runs using independent solutions, both of which produced analogous results (±5%). The hydrodynamic radius, R_H, was calculated assuming a spherical shape, according to the Stokes−Einstein equation, $R_H = k_BT/6\pi\eta D$, where k_B is Boltzmann's constant, T is the temperature, η is the viscosity of the solvent, and D is the experimentally determined diffusion coefficient.

FT-IR Spectroscopy. FT-IR measurements were performed on a Genesis II FT-IR system (Mattson Instruments, Madison, WI). For each spectrum, 250 interferograms were collected with a 4 cm^{-1} resolution. The protein and surfactant were dissolved in buffered D_2O at room temperature for a minimum of 24 h before experimentation. Each sample solution was placed in a demountable liquid cell equipped with CaF_2 windows and a 50 μm Teflon spacer. The sample compartment was continuously purged with CO_2-free dry air for 1 h before data collection to avoid any complication to the spectra from water vapor. IR spectra of solutions without protein were measured under identical conditions and subtracted from the original spectra of solutions containing protein to remove surfactant peaks at ~1600 cm^{-1}. The spectra were Fourier self-deconvoluted with a K factor = 2.0.

UV−Visible Spectroscopy. Absorption measurements were performed on an Agilent (Palo Alto, CA) model 8453 UV−visible spectrophotometer. Cells with a path length of 2 mm were used. When employed, a crystal violet concentration of 10 μM was used. Crystal violet exhibits a maximum absorbance at 590 nm in pure water, far enough away from the azoTAB absorbance (*34*) to be readily detected in azoTAB solutions. The wavelength at which the maximum

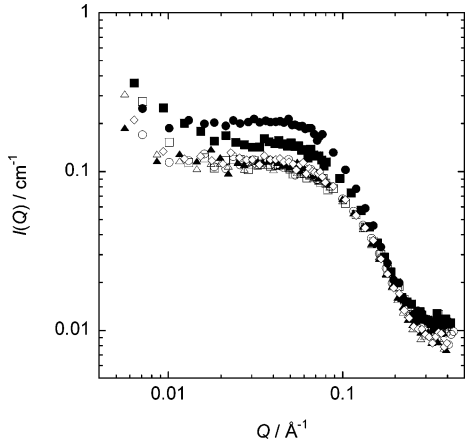

FIGURE 1: SANS data of lysozyme−azoTAB solutions as a function of the surfactant concentration and light illumination. Pure lysozyme (◇), 5.1 mM visible (▲), 5.1 mM UV (△), 7.9 mM visible (■), 7.9 mM UV (□), 12.2 mM visible (●), and 12.2 mM UV (○). [lysozyme] = 11.8 mg/mL.

absorption of crystal violet occurred for each sample was estimated by fitting each absorption spectrum with a fifth-order polynomial.

Fluorescence Spectroscopy. Fluorescence measurements using Nile red as the probe were performed on a Quanta-Master spectrofluorometer model QM-4 (Photon Technology International, Monmouth Junction, NJ) at 25 °C. The results were obtained with an excitation wavelength of 560 nm and an emission wavelength of 650 nm, with excitation and emission slit widths of 4 nm. The spectrofluorometer was loaded with 3 mL of a surfactant−protein solution ([protein] = 10.0 mg/mL), and 30 μL of a 1.0 mM Nile red solution in ethanol was then pipetted into each sample. After this, the samples were stirred for 30 min to reach steady state, as assured by monitoring the change in fluorescence with time. To avoid potential photodegredation of Nile red upon UV light illumination (*41*), when necessary, the lysozyme−azoTAB solutions were pre-exposed to UV light for 2 h before addition of Nile red. UV−visible spectroscopic measurements were then taken immediately following the fluorescence scan to ensure that the surfactant remained in the UV-light form during the course of the measurement.

RESULTS AND DISCUSSION

The ability to control the lysozyme structure with light is shown in the SANS data in Figure 1 as a function of the azoTAB concentration and light illumination. The broad Q range of neutron scattering, in this case $Q = 0.0048-0.46$ Å^{-1}, allows a thorough investigation of protein-folding phenomena by simultaneously investigating a wide range of length scales, $L \propto 2\pi/Q$ ($L = 13.7-1300$ Å). As seen in Figure 1, at a surfactant concentration of either 7.9 or 12.2 mM azoTAB under visible light illumination, the data deviate from the remaining scattering curves beginning at $\sim Q = 0.2$ Å^{-1} or $L = 31$ Å. When compared to the literature value reported for the diameter of lysozyme (~36 Å) (*18*) and to our own value determined by DLS (35 Å, see below), the deviation at this Q value suggests that under visible light azoTAB causes the protein to "swell". However, illuminating these solutions with UV light results in spectra similar to that of pure lysozyme, indicating that the protein refolds back to a size similar to the native state when exposed to UV light.

Table 1: Values of the Radius of Gyration and $I(0)$ Determined from the Guinier Analysis of the SANS Data in Figure 1, as Well as the Protein Maximum Dimension (±3 Å) Obtained from the Pair Distance Distribution Functions

Guinier analysis			PDDF
[surf] (mM)	R_g (Å)	$I(0)$ (cm^{-1})	D_{max} (Å)
0	13.5	0.132	48
Visible Light			
5.1	13.5	0.127	44
7.9	14.3	0.172	48
12.2	14.7	0.228	48
UV Light			
5.1	13.4	0.121	43
7.9	13.2	0.120	42
12.2	13.4	0.118	50

To quantify the effect of light and surfactant on lysozyme folding, Guinier analysis of the SANS data was employed. From the Guinier approximation (*42*), the scattering intensity $I(Q)$ is given by

$$I(Q) = I(0)\exp(-Q^2R_g^2/3) \quad (1)$$

where $I(0)$ is the extrapolated intensity at $Q = 0$ and R_g is the radius of gyration (*43*). Thus, the radius of gyration can be determined from the slope of a plot of $\ln(I(Q))$ versus Q^2 in the region where $QR_g \sim 1$. Values of the radius of gyration calculated in this manner are shown in Table 1. For the "native-like" conformations of pure lysozyme, 5.1 mM surfactant under visible light, and all UV-light surfactant concentrations, the R_g values are in good agreement with the literature value for R_g measured with SANS in D_2O (13.3 Å) (*44*). For 7.9 and 12.2 mM azoTAB under visible light, however, R_g increases to 14.3 and 14.7 Å, respectively. While this roughly 10% increase in the radius of gyration is not as large as the increase observed upon denaturation induced thermally (20%) (*45*) or upon the addition of sodium dodecyl sulfate (30% increase for SDS/lysozyme ~ 300:1, compared to a maximum azoTAB/lysozyme ~ 15:1 in Figure 1) (*17*), urea (40%) (*9*, *14*), or methanol (40%) (*46*), it does, however, support the idea that lysozyme swells under visible light with the azoTAB surfactant and can further refold upon illumination with UV light to a size akin to the native state. Similarly, the radius of gyration of the I_α kinetic intermediate has been observed to be 9% larger than the native state with time-resolved small-angle X-ray scattering experiments upon refolding lysozyme from a GdmCl-unfolded state (*47*).

From the Guinier fits, $I(0)$ was also determined and then used to obtain the molecular weight of the protein to examine the possibility of protein self-association. The weight-average molecular weight of the protein can be determined using the equation

$$I(0) = \frac{M_w c \bar{v}^2 (\rho_p - \rho_s)^2}{N_A} \quad (2)$$

where ρ_s and ρ_p are the scattering length densities of the solvent and protein, respectively, c is the protein concentration, and $\bar{v}$ is the protein-specific volume (*48*). As shown in Table 1, the values of $I(0)$ determined from the data in Figure

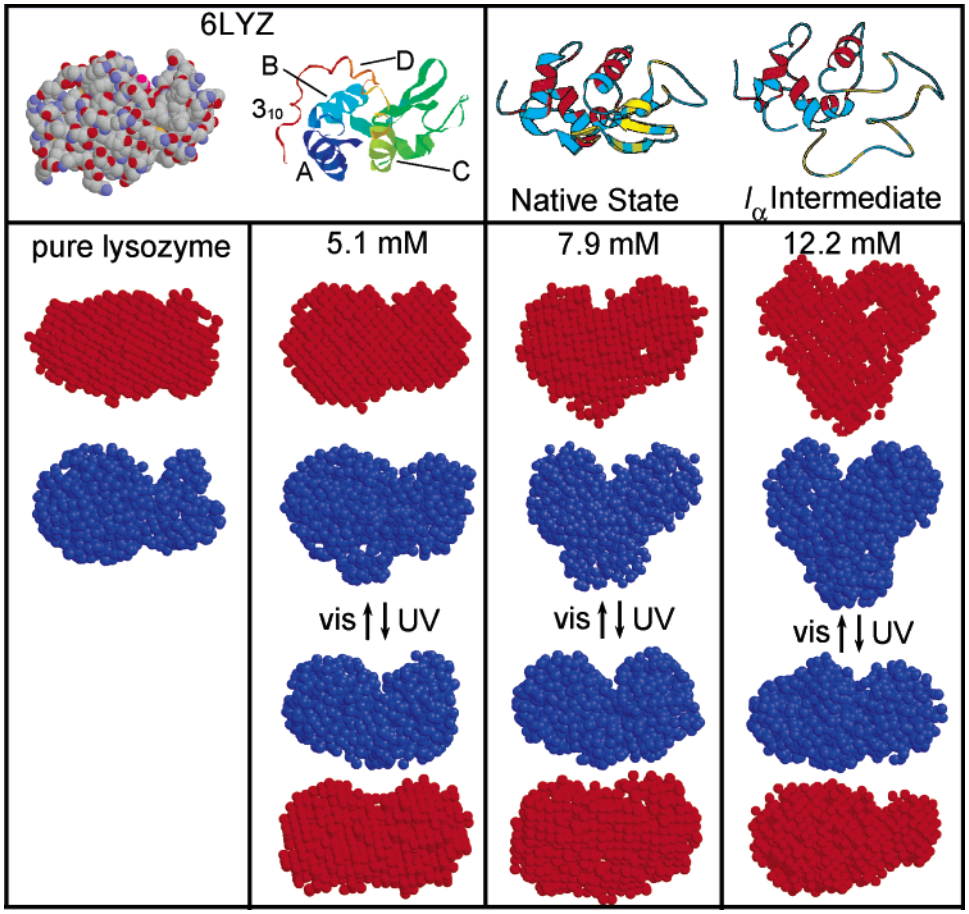

FIGURE 2: Conformation of lysozyme in solution determined from shape reconstruction of the SANS data (best fit in blue, consensus envelope representing the average of 10 runs in red), compared with the X-ray crystallographic structure (*51*) (PDB code 6LYZ). The α domain is shown to consist of helices A (residues 4−15), B (residues 24−36), C (residues 89−99), and D (residues 108−115), along with a 3_{10} helix (residues 120−124) (*26*). Also shown are the structures of the folded state and the I_α intermediate determined from molecular dynamic simulations (*25*). [lysozyme] = 11.8 mg/mL.

1 for the native-like conformations (0.124 ± 0.008 cm^{-1}) agrees nicely with that calculated from the amino acid sequence using the Debye equation [$I(0) = 0.128$ cm^{-1}] (*49*), indicating that self-association does not occur.

The $I(0)$ value is very consistent for all but 7.9 and 12.2 mM under visible light, where an approximately 40 and 80% increase in $I(0)$ is observed, respectively. This increase may appear to indicate protein self-association; however, when considered along with the increase in R_g, it can be seen that this is not the case. For globular proteins (*50*) (see PDDFs below), $R_g \propto M_w^{0.369}$; thus, an 80% increase in the protein average molecular weight (from pure monomer to a mixture of monomer and oligomers) would be expected to result in a 24% increase in R_g, as opposed to the 10% observed. Therefore, the increase in $I(0)$ in Figure 1 does not appear to result from protein association. Instead, this increase in $I(0)$ is likely to be a result of an increase in the effective molecular weight of the surfactant−protein complex [15 or 30 bound surfactant molecules would explain the 40 or 80% increase in $I(0)$, respectively].

While the above results demonstrate that light illumination combined with photoresponsive surfactants can be used to control lysozyme conformation, the values of R_g obtained from the Guinier analysis only provide low-resolution information on the folding process. To gain more insight into this phenomena, a shape-reconstruction algorithm (*37*) was applied to the SANS data by treating the protein as a collection of 1000 scattering centers with positions that are adjusted to the best fit of the data. Shown in Figure 2 are the structures for the runs best fitting each set of data (in blue), along with the resulting "consensus envelopes" (in red) obtained by averaging the 10 runs at each surfactant concentration. Shape-reconstruction techniques require the fitting of the positions of thousands of scatterers with only a few hundred data points; thus, the structures obtained for different runs are not unique and instead depend upon the path of the fits. The consensus envelopes indicate the consistency of the multiple runs.

As seen in Figure 2, all of these shape-reconstruction fits, except 7.9 and 12.2 mM azoTAB under visible light, look very similar in both size and shape and agree quite well with the X-ray crystallographic structure (PDB code 6LYZ) (*51*). This is to be expected because the conformation of soluble proteins in the native state in solution generally agree with the respective crystal structures (*37*, *49*). For lysozyme, this similarity between the solution and crystal structure has been obtained using several techniques such as X-ray and neutron scattering, 2D-NMR, molecular dynamic simulation, differential scanning calorimetry, and laser Raman scattering.

The solution structure determined from the SANS data for pure lysozyme, while not providing for nearly as high of a resolution as X-ray crystallography, does allow the active-site cleft to be observed in the upper right of the molecule between the α and β domains. Furthermore, upon

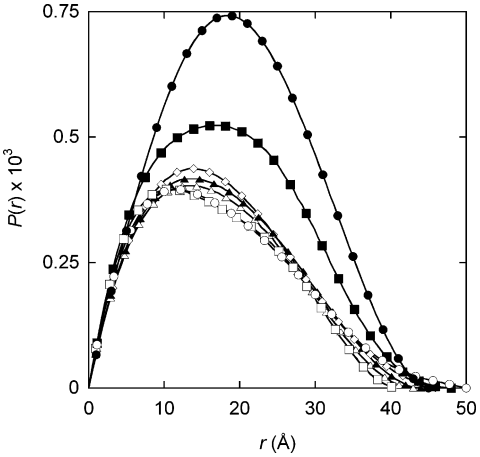

FIGURE 3: PDDFs of lysozyme−azoTAB solutions as a function of the surfactant concentration and light illumination. Pure lysozyme (◇), 5.1 mM visible (▲), 5.1 mM UV (△), 7.9 mM visible (■), 7.9 mM UV (□), 12.2 mM visible (●), and 12.2 mM UV (○). [lysozyme] = 11.8 mg/mL.

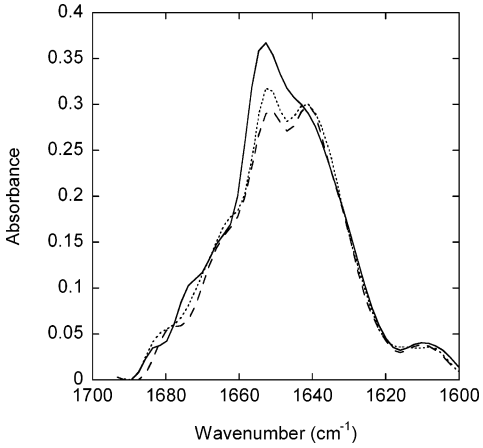

FIGURE 4: Fourier self-deconvoluted FT-IR spectra of lysozyme in the presence of 5.0 mM azoTAB as a function of the light illumination. Pure lysozyme (—), visible (- - -), and UV (•••). [lysozyme] = 10.0 mg/mL.

increasing the surfactant concentration under visible-light illumination, lysozyme is observed to unfold, represented most notably by a progressive swelling of the lower-left side of the protein in Figure 2, although because of rotational averaging as a result of the protein being in solution, it is impossible to assign which domain (α or *β*) is unfolding from the SANS data alone, as will be discussed below.

PDDFs were calculated from the experimental SANS data to further investigate the effects of surfactant and light on the protein structure. A PDDF is the measure of the probability, $P(r)$, of finding two scattering centers (i.e., atomic nuclei) at a distance r apart (*38*, *39*), and calculation of a PDDF from small-angle scattering data is a common method of examining the protein structure (*19*, *52*), providing a simple, model-independent method to probe the myriad of complex structures that proteins can adopt in solution. The results in Figure 3 show that the maximum of the PDDF curve shifts to higher values of r for 7.9 and 12.2 mM azoTAB under visible light. For globular proteins, the maximum of the PDDF (i.e., the most probable dimension) is approximately the protein radius, once again indicating that lysozyme is swollen under visible light for 7.9 and 12.2 mM azoTAB. Furthermore, the PDDF curves at these two concentrations also indicate a higher probability of this most common dimension and are more symmetric about $P(r)_{max}$, implying that the protein−surfactant complex is becoming more "globular" (*19*). Furthermore, the point at which $P(r)$ returns to 0 at large r values defines the maximum dimension within the protein, D_{max}. As shown in Table 1, the D_{max} values for 7.9 and 12.2 mM under visible light are very close to that of pure lysozyme, confirming that the protein does not dramatically elongate but rather "swells" with azoTAB addition. Comparing these model-independent PDDFs to Figure 2 provides a consistency check of the shape-reconstruction analysis. The shape-reconstruction fits show a swelling of the protein, giving rise to the observed increase in r at $P(r)_{max}$, while only a slight increase in the protein length is seen in Figure 2, supported by the fact that the location of D_{max} changes little with surfactant or light and generally agrees with D_{max} for pure lysozyme.

The lack of shoulders or secondary peaks in the calculated pair distance distribution functions also confirm that protein self-association (i.e., the forming of *n*-mers) does not occur. For example, in the case of dimer formation, a secondary peak would develop at an r value equal to the distance between the centers of each monomer, clearly not the case in Figure 3. In terms of larger protein aggregates, a modest increase in the scattering intensity can be seen in Figure 1 at very low Q (<0.01 Å^{-1}), which could possibly indicate the formation of a small amount of such aggregates (*18*). An alternative explanation for this increase could be an imperfect correction of the scattering from the solvent (D_2O), which was also found to exhibit a ∼2-fold increase in scattering intensity below $Q = 0.01$ Å^{-1} [data not shown, see also Svergun and Koch (*53*)]. Note that a slight increase in scattering at low Q has also been observed in similar polyelectrolyte systems (*19*, *49*). Thus, the results obtained from the various techniques used to analyze the SANS data support the conclusion that any aggregation corresponds to a very small fraction of the total lysozyme.

To determine whether Figure 2 represents a swelling of the α or *β* domain of lysozyme, changes in the lysozyme secondary structure were detected with FT-IR spectroscopy in the amide I region (1700−1600 cm^{-1}, due mainly to C═O stretching). Figure 4 shows the FT-IR spectra of pure lysozyme and lysozyme with 5.0 mM azoTAB under both visible and UV light, all in deuterated buffer with 10.0 mg/mL protein. Seven peaks were generally observed in the FSD spectra and assigned to secondary structure elements according to well-established protocols (*54*): 1683 cm^{-1} (*β*-turn), 1674 cm^{-1} (*β*-turn), 1666 cm^{-1} (*β*-turn), 1653 cm^{-1} (α-helix), 1641 cm^{-1} (unordered structures), 1630 cm^{-1} (*β*-sheet), and 1610 cm^{-1} (side chain). Upon the addition of the surfactant, the spectra show a clear decrease in the α-helix peak at 1653 cm^{-1} and a growth in the peak at 1641 cm^{-1} representing unordered structures, while the peaks representing the *β* structures remain relatively unchanged. This indicates that the azoTAB surfactant swells the α domain of the protein, a result of a helix-to-unordered transition. Furthermore, under visible light, the intensity of the peak at 1653 cm^{-1} is smaller than under UV light, indicating that the visible-light form of the surfactant results in a greater degree of unfolding of the α domain. Similar conclusions regarding the surfactant primarily leading to unfolding of the α domain of lysozyme have been observed in the

lysozyme−SDS and lysozyme−cetyltrimethylammonium bromide (CTAB) systems, with the helix-to-unordered transition generally occurring with the addition of 10−40 surfactant molecules/protein at near neutral pH (*55*, *56*), similar to the surfactant/protein ratio in Figure 4 (~7). When the 5.1 mM azoTAB data in Figure 2 is compared with the data in Figure 4, it is clear that changes in the protein secondary structure are observed with FT-IR before significant changes in the tertiary structure (overall shape) are detected with SANS. Furthermore, at azoTAB concentrations higher than 5 mM, there was no observed difference between FT-IR spectra collecting under visible and UV light (data not shown), despite the fact that the SANS data demonstrate considerable changes in the tertiary structure. Similar trends have been observed in the BSA−azoTAB system when comparing SANS and FT-IR data (work in progress).

From Figures 2 and 4, it appears that with the addition of the surfactant the lysozyme adopts an intermediately folded state unique from the I_α intermediate mentioned above. This "surfactant-unfolded intermediate (I_S)" of lysozyme contains a swollen α domain, a likely result of the surfactant tails interacting with protein α-helices, which are generally hydrophobic in nature. Furthermore, by noting the progressive swelling of the lower-left side of the protein in Figure 2 with surfactant addition under visible light, it appears that unfolding of helix A in the α domain may be primarily responsible for formation of the I_S intermediate (with some contribution from helix C also possible). However, it should be cautioned that SANS is an ensemble technique, meaning that if multiple states exist in solution (i.e., a fluctuating intermediate, a mixture of unfolded states, etc.) the structures obtained at 7.9 and 12.2 mM azoTAB under visible light would be considered "average" structures. However, as will be shown below, these structures appear to be true intermediates; thus, when tertiary structures obtained from SANS are combined with the information on the secondary structure from FT-IR, the general mechanism of lysozyme unfolding with the surfactant occurring through denaturing of the α domain can be elucidated.

As the surfactant binds to the protein, hydrophobic interactions between surfactant tails and the nonpolar amino acids occur, allowing these hydrophobic amino acids, which are normally folded within the protein interior, to be exposed to the solvent as the protein swells. For azoTAB, these surfactant−protein interactions can be manipulated with light because the visible-light (trans) form of the surfactant is more hydrophobic than the UV-light (cis) form. This allows for reversible control of lysozyme folding/swelling. Evidence of increased surfactant hydrophobicity influencing protein folding has also been seen in traditional (i.e., nonphotoresponsive) surfactants, where increasing the hydrocarbon tail length for a given headgroup has been shown to result in a greater degree of protein unfolding (*30*).

To study the intermediately folded states of lysozyme that occur with azoTAB addition and light illumination, fluorescence measurements with Nile red as a probe were performed. Nile red is a nonionic and hydrophobic molecule that exhibits low fluorescence in polar media such as water, but when Nile red is preferentially partitioned into nonpolar environments, the molecule will exhibit a large increase in fluorescence. Thus, Nile red fluorescence would be expected

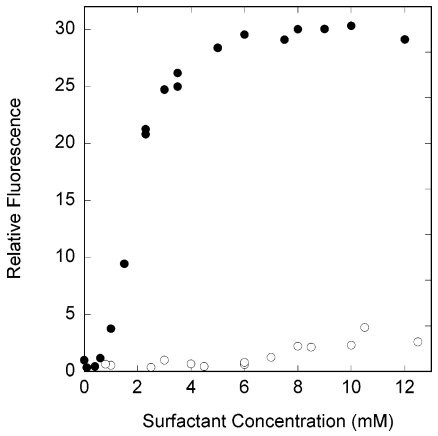

FIGURE 5: Fluorescence of Nile red as a function of the azoTAB surfactant concentration as measured under both visible (●) and UV (○) light illumination. [lysozyme] = 10.0 mg/mL.

to be low in a protein solution with the protein in the native state, because the tightly packed core would prevent Nile red from partitioning into this nonpolar environment. However, if the protein were to swell and the interior of the protein were to become more loosely packed, Nile red could partition into the core, evidenced by an increase in fluorescence. Thus, Nile red fluorescence measurements provide a sensitive technique for differentiating between native and non-native states (*41*). This use of Nile red to probe the formation of hydrophobic domains is conceptually similar to experiments involving ANS, a probe molecule that binds to hydrophobic sites on the protein and has been used to test for the formation of molten globules (*57*). However, the use of ANS ($\lambda_{excite} \sim 400$ nm) is precluded in the present study because of strong absorption of azoTAB at wavelengths less than 500 nm (*34*); thus, Nile red ($\lambda_{excite} \sim 560$ nm) was used.

As seen in Figure 5, for the lysozyme−azoTAB system, the fluorescence of Nile red begins to increase at surfactant concentrations as low as 1 mM and eventually reaches a plateau at around 5 mM under visible light. This indicates that hydrophobic domains become increasingly available for Nile red to partition into the bulk water phase as the surfactant concentration is increased from 1 to 5 mM, despite the fact that the tertiary structure of the protein exhibits only modest differences from the native state over a similar region, as seen in Figure 2. Thus, both FT-IR and fluorescence techniques suggest that a loosely packed protein core develops before the dramatic changes in the protein tertiary structure, observed with SANS. Under UV light, however, the fluorescence of Nile red remains low for all surfactant concentrations, indicating that photoisomerization of the surfactant to the cis form causes lysozyme to refold to a native-like conformation, leading to a decrease in accessible hydrophobic domains.

DLS was also used to investigate the effect of the surfactant and light illumination on the conformation and swelling of lysozyme. As shown in Figure 6a, the measured diffusion coefficients decreased with an increasing surfactant concentration under visible or UV light illumination, indicating an increase in the overall size (hydrodynamic radius) of the protein−surfactant complex. The value obtained for the hydrodynamic radius of pure lysozyme with no surfactant ($R_H = 17.5$ Å) agrees well with literature values ($R_H = 17.4$

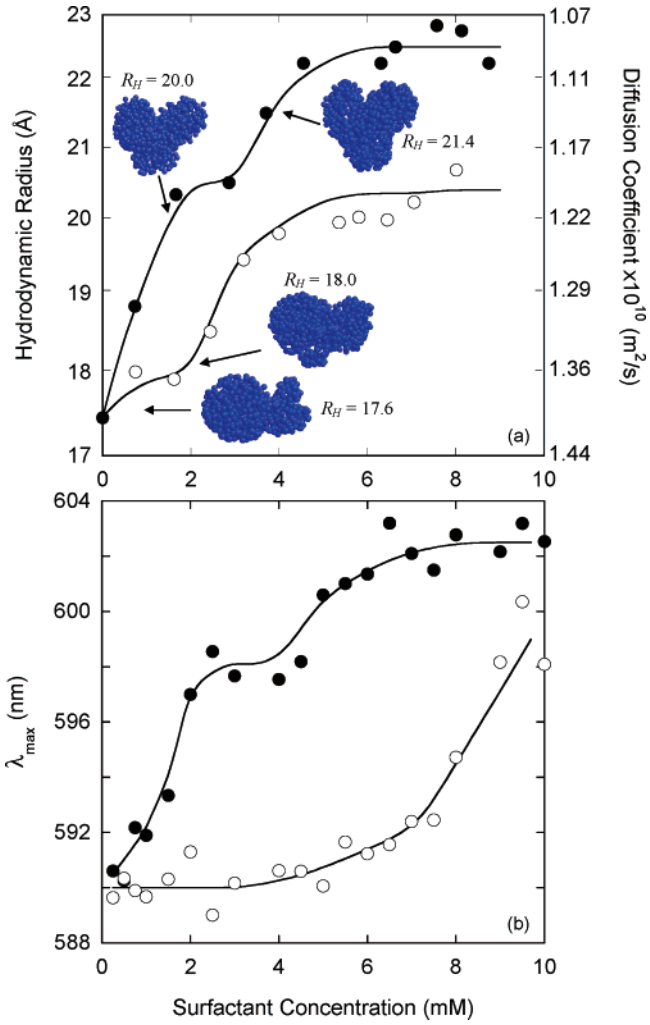

FIGURE 6: (a) Lysozyme swelling as measured by DLS and (b) λ_{max} of crystal violet measured by absorption spectroscopy under both visible (●) and UV (○) light illumination. [lysozyme] = 1.00 mg/mL.

± 0.1 Å) (*17*, *58*) under similar conditions (i.e., low ionic strength, pH ~7).

To compare the light-scattering results in Figure 6a to the SANS fits in Figure 2, estimated hydrodynamic radii (diffusion coefficients) were calculated directly from each shape-reconstruction fit using Kirkwood's theory (*59*) for a collection of spherical subunits. The radius of each subunit was taken to be that of a sphere with a volume of 1/1000th of the molecular volume of lysozyme (1000 scattering centers where used in the shape-reconstruction fits). Water molecules that are tightly bound to the protein−surfactant complex were also accounted for by adding a 3 Å thick water hydration shell to the overall radii (*19*). As seen in Figure 6a, the hydrodynamic properties estimated from the SANS fits agree nicely with the experimental values determined from DLS. Specifically, both SANS and DLS appear to reveal three different protein forms under visible light: a folded (native-like) form at low azoTAB concentrations, a partially folded form at intermediate concentrations, and a swollen/unfolded form at higher azoTAB concentrations.

In the case of neutron scattering, the UV-light form of the surfactant had little to no effect on the conformation of lysozyme, in contrast to Figure 6a. However, the surfactant/protein molar ratio was by necessity much lower for SANS (6.2−14.9) than for DLS (10.5−126), because of the fact that a lower protein concentration was used in the DLS experiments to approximate the diffusion coefficient at infinite dilution. Thus, only one protein conformation is observed with UV-light illumination from SANS data; however, there appear to be at least two forms under UV light from the DLS data, because more surfactant is available to bind to the protein in the case of light scattering. A direct comparison of the SANS and DLS results is therefore not possible, but in general, it is observed that the protein swells with the addition of the visible-light form of the surfactant, while the addition of the UV-light form of the surfactant has a lesser effect. The more hydrophobic, visible-light form of the surfactant has a greater affinity to bind to the protein than the relatively hydrophilic, UV-light form (*19*). Because hydrophobic interactions between surfactant tails and nonpolar amino acids, which are normally folded within the protein interior, allow these amino acids to be exposed to the solvent, protein folding and swelling can be reversibly manipulated with light. This is evident from Figure 6a, because a greater increase in the size of the protein is observed under visible light as opposed to UV light with an increasing surfactant concentration. As previously stated, similar results with conventional (i.e., not photoresponsive) surfactants have shown that a greater degree of protein unfolding occurs in the presence of a more hydrophobic surfactant (*30*). DLS experiments have also been used to examine mixtures of lysozyme and SDS (*16*−*18*). The hydrodynamic radius of the protein−surfactant complex was observed to increase from ~15 to 25 Å as the SDS/lysozyme molar ratio increased from 1.6 to 16.7 (*16*), similar to the results in Figure 6a.

The photoinduced unfolding and refolding of lysozyme observed in this study are consistent with results of the effect of azoTAB and light illumination on BSA conformation (*19*). In the case of BSA, however, a more dramatic unfolding was observed with azoTAB addition, as opposed to swelling in the case of lysozyme. In general, small proteins such as lysozyme are harder to unfold than larger proteins such as BSA, and lysozyme is known to be a tightly folded protein especially in the α domain (*60*), which consists of a hydrophobic pocket enclosed by four helices (although surfactants swell the α domain, as discussed above). Furthermore, the difference in isoelectric points (BSA, pI = 4.7; lysozyme, pI = 11) and net charges [−18 for BSA (*19*) and +8 for lysozyme at neutral pH] may cause binding of the cationic azoTAB to be more difficult in the case of lysozyme and, hence, result in less unfolding. The fact that in this study swelling of lysozyme is observed primarily in the α domain, which contains the aforementioned hydrophobic pocket, demonstrates the importance of hydrophobic surfactant−protein interactions in the unfolding process. Similarly, in solutions of lysozyme mixed with CTAB, hydrophobic interactions were found to dominate over electrostatic repulsion between lysozyme and the positively charged surfactant (*61*).

UV−visible spectroscopy was used to analyze the binding of crystal violet (a nearly planar, cationic probe molecule) to lysozyme. The absorption maximum of crystal violet depends upon the microenvironment in which the probe is located. In a polar solvent such as water, λ_{max} = 590 nm, while in a nonpolar solvent such as benzene, λ_{max} = 605

nm (*62*). Thus, investigating the absorbance of crystal violet upon binding to lysozyme and with the addition of azoTAB allows for the determination of the micropolarity of the local environment surrounding the probe, which can in turn be used to infer about the binding of azoTAB to lysozyme.

As seen in Figure 6b, under visible light, a slight increase in λ_{max} starts at concentrations as low as 0.75 mM azoTAB; however, on average, the λ_{max} values indicate that crystal violet is experiencing a polar environment similar to that of water for surfactant concentrations <2 mM. This demonstrates that there is not yet enough surfactant to dramatically affect the conformation of lysozyme, and crystal violet remains either unbound to lysozyme (likely because both crystal violet and the lysozyme have a positive charge and there is not as strong of a hydrophobic binding force as in azoTAB) or perhaps bound to the surface of the protein (and therefore still exposed to water). Between 2 and 4.5 mM azoTAB under visible light, λ_{max} increases to a nearly constant value of ~598 nm, demonstrating a significant decrease in the local polarity of crystal violet. This is likely a result of protein unfolding/swelling with surfactant addition, which would make normally interior hydrophobic domains of the protein available to crystal violet, combined with the ability of planar crystal violet to "stack" with planar, trans azoTAB molecules bound to the protein. Note that the increase in λ_{max} occurs over similar azoTAB concentrations that an increase in the hydrodynamic radius was observed from DLS, and, furthermore, both sets of data demonstrate a possible plateau in the range of 2−4 mM azoTAB, implying that the lysozyme has adopted a new "partially swollen" form. Increasing the surfactant concentration beyond ~4 mM under visible light causes λ_{max} to again increase, approaching ca. 602 nm, similar in polarity to a benzene-like environment, and indicating that lysozyme has adopted a second "swollen" form. Again, note the similarity in this increase in crystal violet λ_{max} to the increase in the hydrodynamic radius observed over the same surfactant concentrations in Figure 6a. Furthermore, the three protein forms observed in parts a and b of Figure 6 (native-like, partially swollen, and swollen) are consistent with the three forms determined from neutron scattering under visible light (native-like at 5.1 mM azoTAB, partially swollen at 7.9 mM, and swollen at 12.2 mM). Admittedly, the SANS data (11.8 mg/mL) and the DLS and UV−vis data (both at 1.0 mg/mL) are at different protein concentrations; however, the consistency of the results does indicate that the shape-reconstruction fits in Figure 2 demonstrate swelling of the protein.

This decrease in micropolarity observed with crystal violet is not seen with increasing surfactant concentrations under UV light; indeed, λ_{max} stays relatively constant at around 590 nm for concentrations ranging from 0 to 5 mM. At a surfactant concentration of 5 mM under UV light, λ_{max} slowly starts to increase with an increasing surfactant concentration, and above ~6 mM, there appears to be a rapid increase in λ_{max} until a value of ~600 nm is approached. This increase is again at about the same point that the light scattering data demonstrate a plateau, indicating a partially swollen form of lysozyme. Furthermore, beyond this plateau, once the hydrodynamic radius begins to increase again with the surfactant concentration (~8 mM), a steep increase in crystal violet λ_{max} is seen, again similar to the behavior under visible light. The fact that a dampened increase in λ_{max} is observed under UV light compared to visible light is likely a result of the trans (planar) surfactant being more effective at "stacking" with crystal violet, compared to the cis (bent) surfactant form.

CONCLUSION

This study demonstrates that intermediately folded states of lysozyme can be stabilized through the addition of photoresponsive surfactants, thereby allowing lysozyme unfolding and refolding to be controlled with light illumination. The visible-light (trans) form of the surfactant is more hydrophobic than the UV-light (cis) form; hence, surfactant binding to the protein and the protein structure can be tuned with light. Three conformations of the protein were observed under visible light, including a native-like structure at low surfactant concentrations (R_g = 13.5 Å), a partially swollen form at intermediate surfactant concentrations (14.3 Å), and a swollen/unfolded conformation at higher surfactant concentrations (14.7 Å), while UV-light exposure caused the protein to refold. Furthermore, by applying shape-reconstruction methods to SANS data, the precise nature of surfactant-induced protein unfolding was visualized. Combined SANS and FT-IR measurements revealed that lysozyme unfolding occurred primarily in the α domain, potentially initiated by a surfactant-induced denaturing of helix A (residues 4−15). Thus, the surfactant-unfolded conformation appears to represent a folding intermediate unique from the well-known α-domain intermediate of lysozyme that, in contrast, contains a folded α domain and unfolded β domain. The ability to directly track lysozyme unfolding in solution, particularly when combined with photoresponsive surfactants as a means of probing protein structure, illustrates the potential impact of the SANS technique to study protein folding.

ACKNOWLEDGMENT

We thank W. T. Heller for graciously supplying the GA_STRUCT program. We acknowledge the support of the National Institute of Standards and Technology, U.S. Department of Commerce, in providing the neutron research facilities used in this work. This work utilized facilities supported in part by the National Science Foundation under Agreement number DMR-9986442. We also acknowledge the Charles Lee Powell Foundation for support of this research.

REFERENCES

1. Horwich, A. (2002) Protein aggregation in disease: A role for folding intermediates forming specific multimeric interactions, *J. Clin. Invest. 110*, 1221−1232.
2. Dobson, C. M. (1999) Protein misfolding, evolution, and disease, *Trends Biochem. Sci. 24*, 329−332.
3. Morozova-Roche, L. A., Zurdo, J., Spencer, A., Noppe, W., Receveur, V., Archer, D. B., Joniau, M., and Dobson, C. M. (2000) Amyloid fibril formation and seeding by wild-type human lysozyme and its disease-related mutational variants, *J. Struct. Biol. 130*, 339−351.
4. Pepys, M. B., Hawkins, P. N., Booth, D. R., Vigushin, D. M., Tennent, G. A., Soutar, A. K., Totty, N., Nguyen, O., Blake, C. C. F., et al. (1993) Human lysozyme gene mutations cause hereditary systemic amyloidosis, *Nature 362*, 553−557.
5. Valleix, S., Drunat, S., Philit, J.-B., Adoue, D., Piette, J.-C., Droz, D., MacGregor, B., Canet, D., Delpech, M., and Grateau, G. (2002)

Hereditary renal amyloidosis caused by a new variant lysozyme W64R in a French family, *Kidney Int. 61*, 907−912.
6. Bowie, J. U. (2001) Stabilizing membrane proteins, *Curr. Opin. Struct. Biol. 11*, 397−402.
7. Brooks, C. L., III (1998) Simulations of protein folding and unfolding, *Curr. Opin. Struct. Biol. 8*, 222−226.
8. Duan, Y., and Kollman, P. A. (1998) Pathways to a protein folding intermediate observed in a 1-μs simulation in aqueous solution, *Science 282*, 740−744.
9. Jones, J. A., Wilkins, D. K., Smith, L. J., and Dobson, C. M. (1997) Characterization of protein unfolding by NMR diffusion measurements, *J. Biomol. NMR 10*, 199−203.
10. Uversky, V. N., Karnoup, A. S., Segel, D. J., Seshadri, S., Doniach, S., and Fink, A. L. (1998) Anion-induced folding of *Staphylococcal* nuclease: Characterization of multiple equilibrium partially folded intermediates, *J. Mol. Biol. 278*, 879−894.
11. Bachmann, A., Segel, D., and Kiefhaber, T. (2002) Test for cooperativity in the early kinetic intermediate in lysozyme folding, *Biophys. Chem. 96*, 141−151.
12. Yokota, A., Hirai, K., Miyauchi, H., Iimura, S., Noda, Y., Inoue, K., Akasaka, K., Tachibana, H., and Segawa, S. (2004) NMR characterization of three-disulfide variants of lysozyme, C64A/C80A, C76A/C94A, and C30A/C115A−A marginally stable state in folded proteins, *Biochemistry 43*, 6663−6669.
13. Dobson, C. M. (1994) Solid evidence for molten globules, *Curr. Biol. 4*, 636−640.
14. Chen, L., Hodgson, K. O., and Doniach, S. (1996) A lysozyme folding intermediate revealed by solution X-ray scattering, *J. Mol. Biol. 261*, 658−672.
15. Matthews, C. R. (1993) Pathways of protein folding, *Ann. Rev. Biochem. 62*, 653−683.
16. Gimel, J. C., and Brown, W. (1996) A light scattering investigation of the sodium dodecyl sulfate−lysozyme system, *J. Chem. Phys. 104*, 8112−8117.
17. Valstar, A., Brown, W., and Almgren, M. (1999) The lysozyme−sodium dodecyl sulfate system studied by dynamic and static light scattering, *Langmuir 15*, 2366−2374.
18. Stenstam, A., Montalvo, G., Grillo, I., and Gradzielski, M. (2003) Small angle neutron scattering study of lysozyme−sodium dodecyl sulfate aggregates, *J. Phys. Chem. B 107*, 12331−12338.
19. Lee, C. T., Jr., Smith, K. A., and Hatton, T. A. (2005) Photocontrol of protein folding: The interaction of photosensitive surfactants with bovine serum albumin, *Biochemistry 44*, 524−536.
20. Ibel, K., May, R. P., Kirschner, K., Szadkowski, H., Mascher, E., and Lundahl, P. (1990) Protein-decorated micelle structure of sodium-dodecyl-sulfate−protein complexes as determined by neutron scattering, *Eur. J. Biochem. 190*, 311−318.
21. Griko, Y. V., Freire, E., Privalov, G., van Dael, H., and Privalov, P. L. (1995) The unfolding thermodynamics of c-type lysozymes: A calorimetric study of the heat denaturation of equine lysozyme, *J. Mol. Biol. 252*, 447−459.
22. Kiefhaber, T. (1995) Kinetic traps in lysozyme folding, *Proc. Natl. Acad. Sci. U.S.A. 92*, 9029−9033.
23. Matagne, A., Radford, S. E., and Dobson, C. M. (1997) Fast and slow tracks in lysozyme folding: Insight into the role of domains in the folding process, *J. Mol. Biol. 267*, 1068−1074.
24. Radford, S. E., Dobson, C. M., and Evans, P. A. (1992) The folding of hen lysozyme involves partially structured intermediates and multiple pathways, *Nature 358*, 302−307.
25. Dinner, A. R., Sali, A., Smith, L. J., Dobson, C. M., and Karplus, M. (2000) Understanding protein folding via free-energy surfaces from theory and experiment, *Trends Biochem. Sci. 25*, 331−339.
26. Gilquin, B., Guilbert, C., and Perahia, D. (2000) Unfolding of hen egg lysozyme by molecular dynamics simulations at 300 K: Insight into the role of the interdomain interface, *Proteins 41*, 58−74.
27. Booth, D. R., Sunde, M., Bellotti, V., Robinson, C. V., Hutchinson, W. L., Fraser, P. E., Hawkins, P. N., Dobson, C. M., Radford, S. E., Blake, C. C. F., and Pepys, M. B. (1997) Instability, unfolding, and aggregation of human lysozyme variants underlying amyloid fibrillogenesis, *Nature 385*, 787−793.
28. Canet, D., Sunde, M., Last, A. M., Miranker, A., Spencer, A., Robinson, C. V., and Dobson, C. M. (1999) Mechanistic studies of the folding of human lysozyme and the origin of amyloidogenic behavior in its disease-related variants, *Biochemistry 38*, 6419−6427.
29. Shih, P., Holland, D. R., and Kirsch, J. F. (1995) Thermal stability determinants of chicken egg-white lysozyme core mutants: Hydrophobicity, packing volume, and conserved buried water molecules, *Protein Sci. 4*, 2050−2062.
30. Lee, P. K. J., and Jirgensons, B. (1971) Conformational transitions of immunoglobulin fragment Fe(t) incited by alkyl sulfates of various hydrophobic chain lengths, *Biochim. Biophys. Acta 229*, 631−641.
31. Carter, D. C., and Ho, J. X. (1994) Structure of serum albumin, *Adv. Protein Chem. 45*, 153−203.
32. Hayashita, T., Kurosawas, T., Miyata, T., Tanaka, K., and Igawa, M. (1994) Effect of structural variation within cationic azo-surfactant upon photoresponsive function in aqueous solution, *Colloid Polym. Sci. 272*, 1611−1619.
33. Shang, T., Smith, K. A., and Hatton, T. A. (2003) Photoresponsive surfactants exhibiting unusually large, reversible surface tension changes under varying illumination conditions, *Langmuir 19*, 10764−10773.
34. Lee, C. T., Jr., Smith, K. A., and Hatton, T. A. (2004) Photoreversible viscosity changes and gelation in mixtures of hydrophobically modified polyelectrolytes and photosensitive surfactants, *Macromolecules 37*, 5397−5405.
35. Durchschlag, H., Hefferle, T., and Zipper, P. (2003) Comparative investigations of the effects of X- and UV-irradiation on lysozyme in the absence or presence of additives, *Radiat. Phys. Chem. 67*, 479−486.
36. Glinka, C. J., Barker, J. G., Hammouda, B., Krueger, S., Moyer, J. J., and Orts, W. J. (1998) The 30 m small-angle neutron scattering instruments at the National Institute of Standards and Technology, *J. Appl. Crystallogr. 31*, 430−445.
37. Heller, W. T., Krueger, J. K., and Trewhella, J. (2003) Further insights into calmodulin−myosin light chain kinase interaction from solution scattering and shape restoration, *Biochemistry 42*, 10579−10588.
38. Glatter, O. (1977) A new method for the evaluation of small-angle scattering data, *J. Appl. Crystallogr. 10*, 415−421.
39. Feigin, L. A., and Svergun, D. I. (1987) *Structure Analysis by Small-Angle X-ray and Neutron Scattering*, Plenum Press, New York.
40. Svergun, D. I. (1992) Determination of the regularization parameter in indirect-transform methods using perceptual criteria, *J. Appl. Crystallogr. 25*, 495−503.
41. Daban, J. R., Samso, M., and Bartolome, S. (1991) Use of Nile red as a fluorescent probe for the study of the hydrophobic properties of protein−sodium dodecyl sulfate complexes in solution, *Anal. Biochem. 199*, 162−168.
42. Guinier, A., and Fournet, G. (1955) *Small Angle Scattering of X-ray*, Wiley, New York.
43. Gallas, J. M., Littrell, K. C., Seifert, S., Zajac, G. W., and Thiyagarajan, P. (1999) Solution structure of copper ion-induced molecular aggregates of tyrosine melanin, *Biophys. J. 77*, 1135−1142.
44. Stuhrmann, H. B., and Fuess, H. (1976) Neutron small-angle scattering study of hen egg-white lysozyme, *Acta Crystallogr., Sect. A: Found. Crystallogr. 32* (part 1), 67−74.
45. Nicoli, D. F., and Benedek, G. B. (1976) Study of thermal denaturation of lysozyme and other globular proteins by light-scattering spectroscopy, *Biopolymers 15*, 2421−2437.
46. Kamatari, Y. O., Konno, T., Kataoka, M., and Akasaka, K. (1998) The methanol-induced transition and the expanded helical conformation in hen lysozyme, *Protein Sci. 7*, 681−688.
47. Segel, D. J., Bachmann, A., Hofrichter, J., Hodgson, K. O., Doniach, S., and Kiefhaber, T. (1999) Characterization of transient intermediates in lysozyme folding with time-resolved small-angle X-ray scattering, *J. Mol. Biol. 288*, 489−499.
48. Bu, Z., and Engelman, D. M. (1999) A method for determining transmembrane helix association and orientation in detergent micelles using small-angle X-ray scattering, *Biophys. J. 77*, 1064−1073.
49. Velev, O. D., Kaler, E. W., and Lenhoff, A. M. (1998) Protein interactions in solution characterized by light and neutron scattering: Comparison of lysozyme and chymotrypsinogen, *Biophys. J. 75*, 2682−2697.
50. Uversky, V. N. (1993) Use of fast protein size-exclusion liquid chromatography to study the unfolding of proteins which denature through the molten globule, *Biochemistry 32*, 13288−13298.
51. Diamond, R. (1974) Real-space refinement of the structure of hen-egg-white lysozyme, *J. Mol. Biol. 82*, 371−391.

52. Ibel, K., May, R. P., Kirschner, K., Szadkowski, H., Mascher, E., and Lundahl, P. (1990) Protein-decorated micelle structure of sodium-dodecyl-sulfate−protein complexes as determined by neutron scattering, *Eur. J. Biochem. 190*, 311−318.
53. Svergun, D. I., and Koch, M. H. J. (2003) Small-angle scattering studies of biological macromolecules in solution, *Rep. Prog. Phys. 66*, 1735−1782.
54. Fabian, H., and Mantele, W. (2002) in *Handbook of Vibrational Spectroscopy* (Chalmers, J. M., and Griffiths, P. R., Eds.) pp 3399−3424, Wiley, New York.
55. Lad, M. D., Ledger, V. M., Briggs, B., Green, R. J., and Frazier, R. A. (2003) Analysis of the SDS−lysozyme binding isotherm, *Langmuir 19*, 5098−5103.
56. Liu, H., Yang, W., and Chen, J. (1998) Effects of surfactants on emulsification and secondary structure of lysozyme in aqueous solutions, *Biochem. Eng. J. 2*, 187−196.
57. Semisotnov, G. V., Rodionova, N. A., Razgulyaev, O. I., Uverskii, V. N., Gripas, A. F., and Gil'manshin, R. I. (1991) Study of the "molten globule" intermediate state in protein folding by a hydrophobic fluorescent probe, *Biopolymers 31*, 119−128.
58. Colvin, J. R. (1952) Size and shape of lysozyme, *Can. J. Chem. 30*, 831−834.
59. Kirkwood, J. G. (1996) The general theory of irreversible processes in solutions of macromolecules, *J. Polym. Sci. Pol. Phys. 34*, 1−14.
60. Yokota, A., Hirai, K., Miyauchi, H., Iimura, S., Noda, Y., Inoue, K., Akasaka, K., Tachibana, H., and Segawa, S.-i. (2004) NMR characterization of three-disulfide variants of lysozyme, C64A/C80A, C76A/C94A, and C30A/C115A−A marginally stable state in folded proteins, *Biochemistry 43*, 6663−6669.
61. Chatterjee, A., Moulik, S. P., Majhi, P. R., and Sanyal, S. K. (2002) Studies on surfactant−biopolymer interaction. I. Microcalorimetric investigation on the interaction of cetyltrimethylammonium bromide (CTAB) and sodium dodecyl sulfate (SDS) with gelatin (Gn), lysozyme (Lz), and deoxyribonucleic acid (DNA), *Biophys. Chem. 98*, 313−327.
62. Mackay, R. A., Letts, K., and Jones, C. (1977) in *Micellization, Solubilization, and Microemulsions* (Mittal, K. L., Ed.) pp 801, Plennum, New York.

BI051646C